JGR Space Physics

RESEARCH ARTICLE
10.1029/2022JA030930

Key Points:

- First study on a new concept of a multi-frequency high-frequency (HF) beacon for the direct measurement of D-region absorption is presented
- Full physics-based model of HF radio absorption in the upper atmosphere is developed
- A machine learning model is developed and the capability of the model in estimation of D and E-region constituents is examined

Correspondence to:
A. Mahmoudian,
a.mahmoudian@ut.ac.ir

Citation:
Mahmoudian, A., Kosch, M. J., & Baghaei, R. M. (2023). Global simulations of multi-frequency HF signal absorption for direct observation of middle atmosphere temperature and composition. *Journal of Geophysical Research: Space Physics*, *128*, e2022JA030930. https://doi.org/10.1029/2022JA030930

Received 15 AUG 2022
Accepted 3 JAN 2023

Author Contributions:
Conceptualization: Alireza Mahmoudian
Data curation: Reza Mohammadi Baghaei
Formal analysis: Alireza Mahmoudian
Investigation: Alireza Mahmoudian
Methodology: Alireza Mahmoudian
Software: Alireza Mahmoudian
Supervision: Alireza Mahmoudian
Validation: Alireza Mahmoudian
Writing – original draft: Alireza Mahmoudian
Writing – review & editing: Michael J. Kosch

Global Simulations of Multi-Frequency HF Signal Absorption for Direct Observation of Middle Atmosphere Temperature and Composition

Alireza Mahmoudian[1], Michael J. Kosch[2,3,4], and Reza Mohammadi Baghaei[1]

[1]Institute of Geophysics, University of Tehran, Tehran, Iran, [2]Department of Physics, Lancaster University, Lancaster, UK, [3]South African National Space Agency (SANSA), Hermanus, South Africa, [4]Department of Physics and Astronomy, University of the Western Cape, Bellville, South Africa

Abstract This paper presents the first numerical study on a new concept for the direct measurement of D-region absorption in the high-frequency (HF) band. Numerical simulations based on the Appleton-Hartree and Garrett equations of refractive index are presented. Electron temperature as a result of HF radio pumping of the ionosphere is included in the calculations using proper numerical formulation. Both O- and X-mode radio wave polarizations are taken into consideration. A global map of HF absorption in the northern hemisphere is calculated. Detailed calculations of HF radio wave absorption as it propagates through the lower atmosphere are presented. The effect of several parameters on the amount of absorption is calculated. The best frequencies to be used for the purpose of this study are discussed. A machine learning model is developed and the capability of the model in estimation of D and E-region constituents includes N_2, O, O_2, as well as T and N_e is examined. Such a technique can also lead to global mapping of HF absorption and improve OTHR (over-the-horizon-radar) performance.

1. Introduction

The lower atmosphere has a great impact on the propagation of high-frequency (HF) radio waves. These effects could result in distortion of the HF signal and may limit the applications of this frequency band specifically for remote sensing applications. Remote sensing of the ionosphere and ionospheric tomography has been an area of great interest amongst space physicists. Satellite-based ionospheric tomography using beacons as well as satellite radio signal transmission and ground reception has been studied over the past several decades. There are ground-based instruments such as riometers, radio receivers that continuously monitor the power received from extraterrestrial radio sources (Little & Leinbach, 1959), which are designed to measure D-region absorption. While using a higher operating frequency for riometers (VHF band) may reduce the sensitivity to absorption, these signals must pass through the ionosphere, and they are subject to varying attenuation due to changes in the electron density.

The first use of beacons on rockets for measuring ionospheric parameters was carried out by Seddon (1953). The first mission had continuous wave radio transmissions from the rocket at HF frequencies (4.27 MHz or 7.75 MHz and their sixth harmonic). Further details on ionospheric layer profiling using rocket beacon signals are described by Bernhardt et al. (1993), Evans (1977), Friedman (1959), Jackson (1954), Maeda (1970), Seliga, 1968, and Smith and Gilchrest (1984).

The Naval Research Laboratory has developed a Coherent Electromagnetic Radio Tomography beacon with frequencies at VHF (150 MHz) and UHF (400 MHz) in collaboration with the Air Force Research Laboratory (AFRL). The developed CETRO beacon has been used on the Communications/Navigation Outage Forecast System satellite (de La Beaujardie're et al., 2004) to register low-latitude scintillations recorded by the AFRL Scintillation Decision Aid network of ground receivers (Bernhardt et al., 1998; Bernhardt et al., 2001; Bernhardt et al., 2005; Bernhardt & Siefring, 2006; Caton et al., 2004; Groves et al., 1997). Bernhardt and Huba (1993) and Bernhardt et al. (1993) developed numerical simulations, known as computerized ionospheric tomography, which can reconstruct images of F-region irregularities.

Heating of the ionospheric plasma by modulated HF waves leads to physical processes with a wide range of scales due to an elevated T_e/T_i (electron to ion temperature). Artificial modulation of the D-region plasma to diagnose dusty plasma associated with polar mesospheric summer echoes has been an area of research over the

past two decades (Havnes, 2004; Mahmoudian et al., 2020; Scales, 2004; Scales & Mahmoudian, 2016). Polar mesospheric summer echoes (PMSE) are strong radar echoes associated with polar mesospheric clouds, which are natural ice/dust layers in the polar region in the altitude range of 80–90 km and are widely believed to be a direct manifestation of global warming. A remote sensing technique has been developed to study this region during modulation by high-power radio waves using multi-frequency radar observations. Our recent work has shown that the modified ionosphere can lead to enhanced absorption of radio waves in the ionosphere. The estimated D-region absorption at 8 MHz has been studied to observe the PMSE (Senior et al., 2011, 2014).

The idea of implementing a multi-frequency radio beacon in low Earth orbit has been used for many years to study ionospheric irregularities through the scintillation information of the signal passing through the ionosphere using GPS signals. The present work describes the general idea of developing a multi-frequency HF beacon to be used for measuring various ionospheric and upper atmosphere parameters. The basic idea is to develop the first multi-frequency HF beacon to fly on a CubeSat in order to obtain the first direct measurement of D-region parameters. Other applications of Iran's first CubeSat mission with multi-frequency HF beacon (REEIMA: Radio Explorer for Earth, Ionosphere, Mesosphere, and Atmosphere) to measure ionospheric, mesospheric, and atmospheric parameters are introduced. Specifically, the frequency selection for the HF beacon is considered by including a detailed computational model of HF absorption in the D-region. The absorption model is capable of calculating the loss rate associated with vibrational and rotational cooling of electrons due to the presence of neutral atoms. The ionospheric model, including the Appleton-Hartree and Garrett equations of refractive index, is considered. The model is also designed to calculate the absorption and enhanced electron temperature in the presence of mesospheric conditions modulated by high-power HF radio waves. A machine learning (ML) model is developed and the capability of the model in estimating D and E-region constituents N_2, O, O_2, as well as T and N_e, is introduced. Discussion on remote sensing of mesospheric parameters based on the simulation results is provided.

2. Computational Model

The model used in this study includes a general expression of electron temperature enhancement in the presence of an HF radio wave transmitted from the ground. This expression, which includes the time variation of electron temperature, can be written as follows:

$$\frac{3}{2}k_B N_e \frac{dT_e}{dt} = -2S(t)\frac{\omega}{c}\mathrm{Im}\mu(N_e, T_e) - N_e L(T_e, T_n) \tag{1}$$

where k_B is Boltzmann's constant, N_e, T_e are the electron number density and temperature, w is the disturbing wave angular frequency, c is the free space speed of light, m is the complex refractive index of the disturbing wave and L (T_e, T_n) is the electron energy loss function where T_n is the neutral gas temperature. O_2, N_2, and O neutral gases are considered here. The first term on the right represents the energy gained by electrons due to the absorption of the pump wave. This equation includes the time varying power flux $S(t)$, which modifies the background electron temperature in the interaction region. The model is set up such that the ordinary Appleton-Hartree formula and generalized refractive index of Garrett (1985) can be implemented in the calculations. One of the main features that make this model distinct, in comparison with other time dependent heating models, is the inclusion of self-absorption of the high-power HF heating wave. One of the practical ways to measure the absorption coefficient is to send a low power HF pulse and high-power HF heating wave in alternating sequences. The high-power HF pulse modifies the background electron density and temperature in the D-region and enhances the absorption coefficient. Therefore, such an experimental set up can be used to measure the natural absorption in the absence of an heating signal as well as in the modified mesospheric conditions.

2.1. Refractive Index

The electromagnetic wave propagation in different materials and the environment is mostly governed by refractive index of the local region. The Appleton-Hartree equation of refractive index, which can be written in the following form, describes the propagation of electromagnetic waves in a cold and magnetized plasma:

$$\mu^2 = 1 - \frac{X}{1 - Iz\frac{\frac{1}{2}Y^2\sin^2\theta}{1-X-iZ} \pm \frac{1}{1-X-iZ}\left(\frac{1}{4}Y^4\sin^4\theta + Y^2\cos^2\theta(1-X-iZ)\right)} \tag{2}$$

where $X = \left(\omega_0^2\right)/\omega^2, Y = \omega_{ce}/\omega, Z = \nu/\omega, \omega$ denotes the frequency of the propagation signal, ω_0 is the electron plasma frequency, Ω_{ce} is the electron gyro-frequency, θ represents the angle between the ambient magnetic field vector and the wave vector, and ν is the electron-neutral collision frequency. It should be noted that these parameters vary with altitude. From this expression, radio wave propagation in the ionosphere in the presence of cold magnetized plasma will depend on the direction of propagation relative to the background magnetic field, transmission frequency as well as background ionospheric parameters. It should be noted that the generalized refractive index of Garrett (1985, 1991) has also been implemented in the model. A full discreption of the Garrett model is provided in Appendix A. It will be shown that the difference between Appleton-Hartree and Garrett's refractive index in estimating HF radio wave absorption is less than ~0.03 dB/km. A comparison of the results obtained using the two models is provided in the following sections.

2.2. Cooling Model

Studying the electron temperature variation in the ionosphere requires a good insight to a possible heating, cooling, and energy flow processes under natural or artificially modified conditions. The enhanced electron temperature, as a result of external HF pump heating, could be reduced due to the cooling of the electrons by neutral particles present in this region. The cooling process is mainly due to the vibration or rotational collisions of electrons with neutral particles. The cooling efficiency varies significantly with the type of neutral atoms. The major neutral particle densities and temperature of N_2, O_2, and O in this region are imported from the NRLMSISE-00 model. The main neutral atoms and cooling processes used in this study are the vibrational and rotational cooling of electrons by N_2 and O_2 atoms.

The cooling rate (loss rate) for the N_2 atom and due to rotational excitation can be written as (Schunk & Nagy, 1978) (SN78):

$$L = 2.9e \times 10^{-20} N_e \times N_2(T_e - T_n)/\sqrt{T_e} \tag{3}$$

where L is the loss rate, n_e is the electron density, N_2 is the density of Nitrogen atoms, T_n is the neutral temperature, T_e is the electron temperature. The cooling rates for O_2, using Pavlov's expression, can be as follow (Pavlov, 1998a, 1998b, 1998c):

$$L = 6.9e \times 10^{-20} N_e \times O_2(T_e - T_n)/\sqrt{T_e} \tag{4}$$

According to Pavlov (1998c) the N_2 rotational excitation is similar to SN78 with a correction factor of 1.255, which is considered in this study. The cooling rates based on Pavlov (1998a, 1998b, 1998c) are referred to as P98 in the text. The vibrational cooling by N_2 can be written, using the SN78 formula, as:

$$f = 1.06 \times 10^4 + 7.51 \times 10^3 \times \tanh\left(1.10 \times 10^{-3}(T_e - 1800)\right) \tag{5}$$

$$g = 3300 + 1.233 \times (T_e - 1000) - 2.056 \times 10^{-4} \times (T_e - 1000)(T_e - 4000) \tag{6}$$

$$L = 2.99e \times 10^{-18} N_e N_2 \times e^{\left(\frac{f(T_e - 2000)}{2000 T_e}\right)}\left(1 - e^{-\frac{g(T_e - T_n)}{(T_e T_n)}}\right) \tag{7}$$

The vibrational cooling by N_2 using P98 can be written as:

$$\begin{aligned} L = N_e N_2 \Bigg[\left(1 - e^{-3353/T_{vib}}\right) \times \sum_{v=1}^{10} Q_{0v}\left(1 - e^{\left[v3353\left(T_e^{-1} - T_{vib}^{-1}\right)\right]}\right) + \\ \left(1 - e^{-3353/T_{vib}}\right) e^{-3353/T_{vib}} \times \sum_{v=2}^{9} Q_{1v}\left(1 - e^{\left[(v-1)3353\left(T_e^{-1} - T_{vib}^{-1}\right)\right]}\right)\Bigg] \end{aligned} \tag{8}$$

where T_{vib} is assumed to be equal to T_n. Q_{0v} and Q_{1v} (the electron energy transfer rates) are calculated for $T_e > 1{,}500$ and $T_e \leq 1{,}500$, respectively, and based on coefficients provided in Tables 2 and 3 of Pavlov (1998a).

The vibrational cooling by O_2 can be written as (Schunk & Nagy, 1978) (SN78):

$$h = 3300 - 839 \times sin\left(1.91 \times 10^{-4} \times (T_e - 2700)\right) \tag{9}$$

$$L = 5.19e \times 10^{-19} N_e O_2 \times e^{\frac{h(T_e-700)}{(700T_e)}} \left(1 - e^{\frac{-2770(T_e-T_n)}{T_e T_n}}\right) \quad (10)$$

The O_2 rotational excitation from SN78 is given by:

$$L = 5e \times 6.9 \times 10^{-20} \times (N_e O_2 (T_e - T_n))/\sqrt{T_e} \quad (11)$$

O_2 rotational excitation and cooling rate (Pavlov, 1998a) (P98) is given by:

$$L = 5.2e \times 10^{-21} \times \frac{N_e O_2 (T_e - T_n)}{\sqrt{T_e}} \quad (12)$$

O_2 vibrational excitation is based on expressions 1–5 and Table 1 in Jones et al. (2003) (J03). The calculation of N_2 vibrational excitation is from Campbell et al. (2004) (C04).

Three scenarios are considered for the combination of cooling rates shown in expressions (3–12). In the standard scenario, N_2 vibrational and rotational excitation and N_2 rotational cooling using the P98 formulation and O_2 vibrational excitation using the J03 formula is used. The Standard-04 cooling model based on N_2 and O_2 rotational excitation using the P98 model, O_2 vibrational excitation using the J03 formula, and N_2 vibrational cooling using the C04 is implemented. The Stubbe cooling model based on N_2 and O_2 rotational and vibrational excitation, obtained using SN78, is used. A close comparison of three scenarios on the associated estimated HF absorption will be examined in the following sections. The main concept to investigate in Section 2 is to evaluate available theories for cooling models, and to explore their impact on the absorption calculation versus altitude at different transmission frequencies. This is a critical step to show that model is robust for different estimations included in the cooling rate formulations. As it will be shown later in the paper, the degree of variation in the absorption results, based on the three cooling models proposed in this paper, is negligible.

3. Numerical Results

The numerical solution of electron temperature variation is considered to calculate the electron temperature enhancement during radio wave heating of the ionosphere as well as the modified electron-neutral collision frequency. The amount of signal absorption as a function of electron temperature can be obtained from:

$$S_{out}(t) = \left(\frac{z}{z + \Delta z}\right)^2 S(t) + 2S(t)\Delta z \frac{\omega}{c} \mathrm{Im}\mu(N_e, T_e) \quad (13)$$

In this approach the region of interest can be divided to small sections with a thickness of Δz. The input power is $S(t)$ and the output power at the end of each section, including the absorbed signal, is shown by $S_{out}(t)$. The value of output power at each altitude is calculated with a delay to include the absorption in the lower layers.

Several parameters are used in this study such as the polarization of the transmitted signal (O- and X-mode) and transmission frequency in the range of 2–30 MHz for both the natural and artificially modified ionosphere. The main goal of this study is to determine the characteristics of the signal within the HF band to develop a remote sensing technique to measure absorption in the D-region. This approach and the selected frequencies will be used to design a future CubeSat mission (REEIMA: Radio Explorer for Earth, Ionosphere, Mesosphere, and Atmosphere). The main idea is to design a multi-frequency HF beacon to fly on first Iran's CubeSat and to measure ionospheric, mesospheric, and atmospheric parameters. The basic changes of a signal passing through the ionosphere, including absorption, scattering, diffraction, amplitude and phase scintillation, Faraday rotation, spectral Doppler shift, will be used to determine the basic parameters of the ionosphere and mesosphere. The REEIMA CubeSat mission is designed to be used for other applications such as gravity wave characterization. The review of the mission and applications are beyond the scope of the current paper and will be discussed in more detail elsewhere.

Figure 1a presents a comparison of the HF absorption profile at 8 MHz obtained using the Garrett and AH refractive indices. Figure 1a presents the absorption profile for unheated and heated (elevated T_e/T_i) conditions. Blue and black lines show the O- and X-mode results. The main difference between Garrett and AH formulation of refractive index appears near the maximum amplitude. The difference in predicted values of total absorption

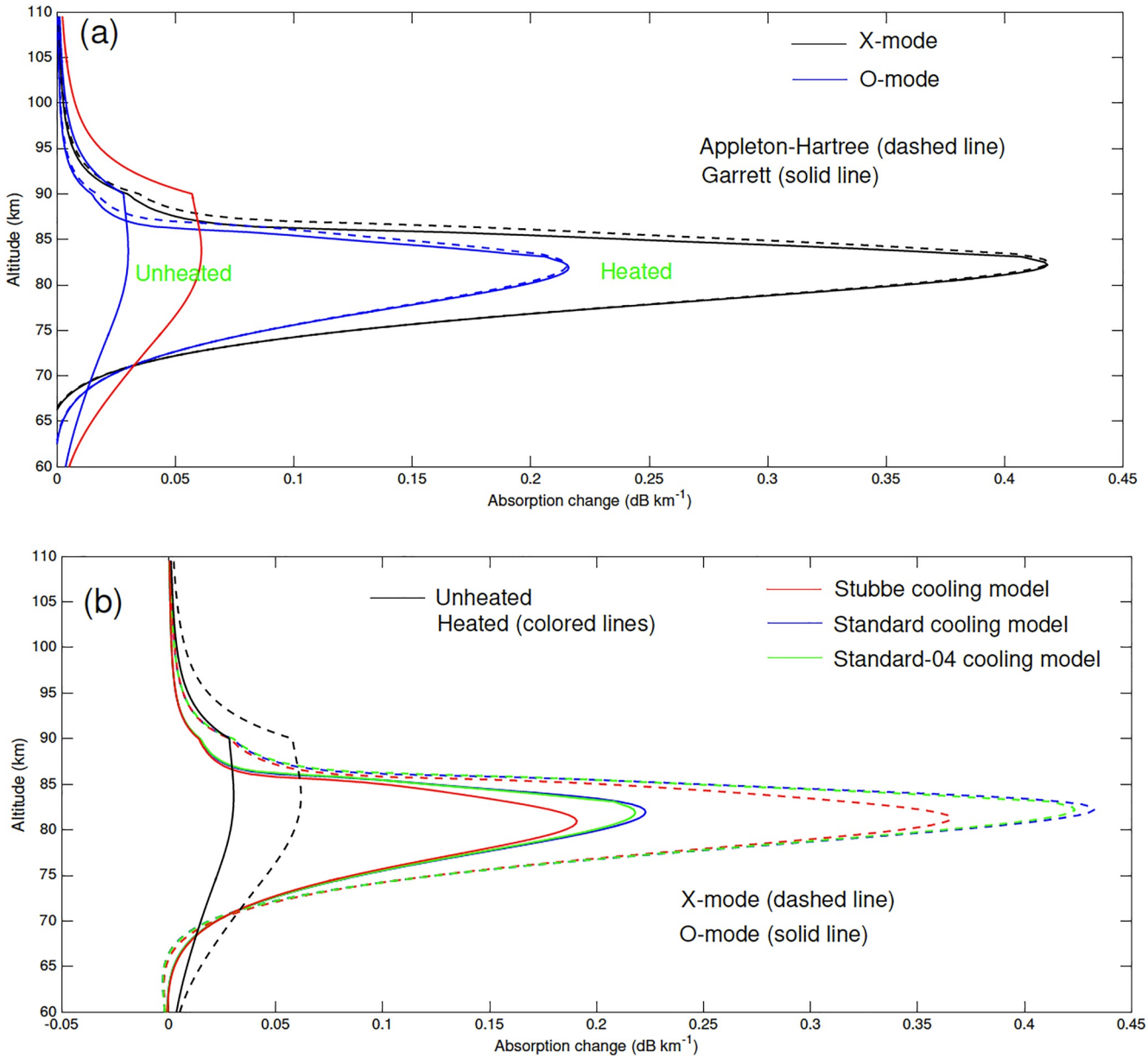

Figure 1. (a) O-mode and X-mode absorption versus altitude obtained using Appleton-Hartree formula for the refractive index assuming phase propagation parallel to the magnetic field and Garrett's generalized refractive index formula in the heated and unheated D-region. (b)The effect of different cooling models on the calculated absorption amplitude of the (a) unheated and (b) heated ionosphere. The transmission frequency of 8 MHz is considered.

is similar for both ionospheric conditions (and at each transmission frequency). Total HF absorption associated with Figure 1a is provided in Table 2. According to Table 2, the difference between the estimated total absorption is of order 0.032 dB (0.07 dB) for O-mode (X-mode) in the unheated ionosphere. A similar calculations for heated ionosphere show a total absorption of 0.24 dB (0.42 dB) for O-mode (X-mode). The results show that the refractive index model used in the calculations has a minimal effect on the absorption estimates. Moreover, implementing HF absorption measurements at multi-frequency in heated and unheated conditions would result in the calibration of the instrument and accurate determination of ionospheric constituents.

Detailed investigation of the cooling rate models presented in Table 1, is provided in Figure 1b. O-mode and X-mode absorption versus altitude is shown using Appleton-Hartree formula for the refractive index assuming phase propagation parallel to the magnetic field and Garrett's generalized refractive index formula in the heated and unheated D-region. The transmission frequency of 8 MHz is shown. Three cooling models associated with N_2

Table 1
The Cooling Rates Used in This Study Based on the Combination of Rates for Vibrational and Rotational N_2 and O_2 Using SN78 (Schunk & Nagy, 1978), P98 (Pavlov, 1998a), J03 (Jones et al., 2003) and C04 (Campbell et al., 2004) Calculations

Cooling approach	Standard	Standard 04	Stubbe
Cooling rates	N_2 Vibrational P98	N_2 Vibrational C04	N_2 Vibrational SN78
	N_2 Rotational P98	N_2 Rotational P98	N_2 Rotational SN78
	O_2 Vibrational J03	O_2 Vibrational J03	O_2 Vibrational SN78
	O_2 Rotational P98	O_2 Rotational P98	O_2 Vibrational SN78

and O_2 vibrational and rotational cooling are used. The calculated HF absorption profile associated with Stubbe, Standard, and Standard-04 cooling models are presented in green, blue, and black colors, respectively. According to Figure 1b, no change in HF absorption profile is seen for different cooling models used in this paper. Both O- and X-mode absorption profiles at 8 MHz are consistent with various cooling rates included. For heated plasma conditions, the HF absorption profiles show a small discrepancy as shown in Figure 1b. The difference between the predicted absorption profile using Standard and Standard-04 cooling models is negligible for both O- and X-modes. Considering the possibility of conducting HF absorption measurements in a short amount of time (to probe the region of D- and E-regions) under heated and unheated ionospheric conditions, the best cooling model to fit the observations can be determined in the future coordinated experiments. As shown in Figure 1b, the cooling models are more sensitive to background electron temperature. Therefore, the best cooling model appropriate for modified ionosphere is required to be determined before further analysis and ML can be applied to determine background atmospheric parameters. The proposed experiment set up and observations are a necessary step for the data calibration and selection of accurate cooling model. This is beyond the scope of this manuscript.

Typical variation of the HF absorption profile versus altitude is shown in Figure 2. The electron density profile is assumed to increase linearly from 60 to 90 km (10^7–10^{10} m^{-3}). A constant electron density of 10^{10} m^{-3} is assumed for altitude range of 90–110 km. The region is zoomed, in comparison with previous figures, to show the detailed variation of the absorption profiles. HF frequencies of 3, 8, 14, 21, and 28 MHz are used. A typical electron temperature profile (Figure 2b) is used. A substantial reduction in maximum absorption amplitude is seen as the frequency decreased from 8 to 3 MHz. The figures show that the maximum absorption is mainly limited to the altitude range of 75–95 km. This altitude range increases for the X-mode. The X-mode reveals a larger variation concerning the higher frequencies used in this study. Another interesting change observed in Figures 2d and 2e is the negative effect of HF pump heating (increased T_e/T_i) on the absorption profile at low frequencies and altitudes below 75 km. A more detailed study of the results is provided in Table 3 based on the measurable parameters in the actual experiment.

Table 3 represents the total absorption of O-mode and X-mode in the unheated and heated D-region as well as the total phase variation of the propagating signal at 3, 8, 16, 24, and 28 MHz. The absorption amplitude in dB per kilometer (dB km^{-1}) is shown for different altitudes from 60 to 110 km. According to this Table, the maximum total absorption is 1.9, 0.454, 0.17, 0.082, and 0.048 dB, as the frequency changes from 3 to 28 MHz. These values for the X-mode are ~12, 0.89, 0.256, 0.1, and 0.059 dB for transmission frequencies of 3, 8, 16, 24 (and 28) MHz, respectively. The close comparison of the absorption value for the O-mode and X-mode shows that this technique along with five-implemented frequencies has a unique signature and can be used to determine the mesospheric parameters based on the amount of absorption. Considering the predictable scale of absorption at the selected frequency bands, the received signal on the ground can also be corrected to the original amplitude. The corrected signal then can be used for other applications such as deriving the scintillation parameters to determine ionospheric irregularities.

Table 2
Total High-Frequency Absorption Associated With the Results Presented in Figure 1

	Absorption O-mode	Absorption X-mode	Phase O-mode	Phase X-mode
Garett's generalized refractive index formula				
Unheated	0.422	0.825	4173.755	4173.267
Heated	2.175	3.816	4173.861	4173.501
Appleton-Hartree formula for the refractive index				
Unheated	0.454	0.894	4173.753	4173.264
Heated	2.421	4.238	4173.871	4173.529

Note. The calculations are made using Garrett and AH formula of refractive index. Unheated and artificially modulated ionosphere using HF radio waves are considered.

3.1. Neutral Density

Another parameter that has been investigated in this study is the effect of neutral density variation on the absorption at different transmission frequencies, in the artificially modified as well as the natural D-region condition, the

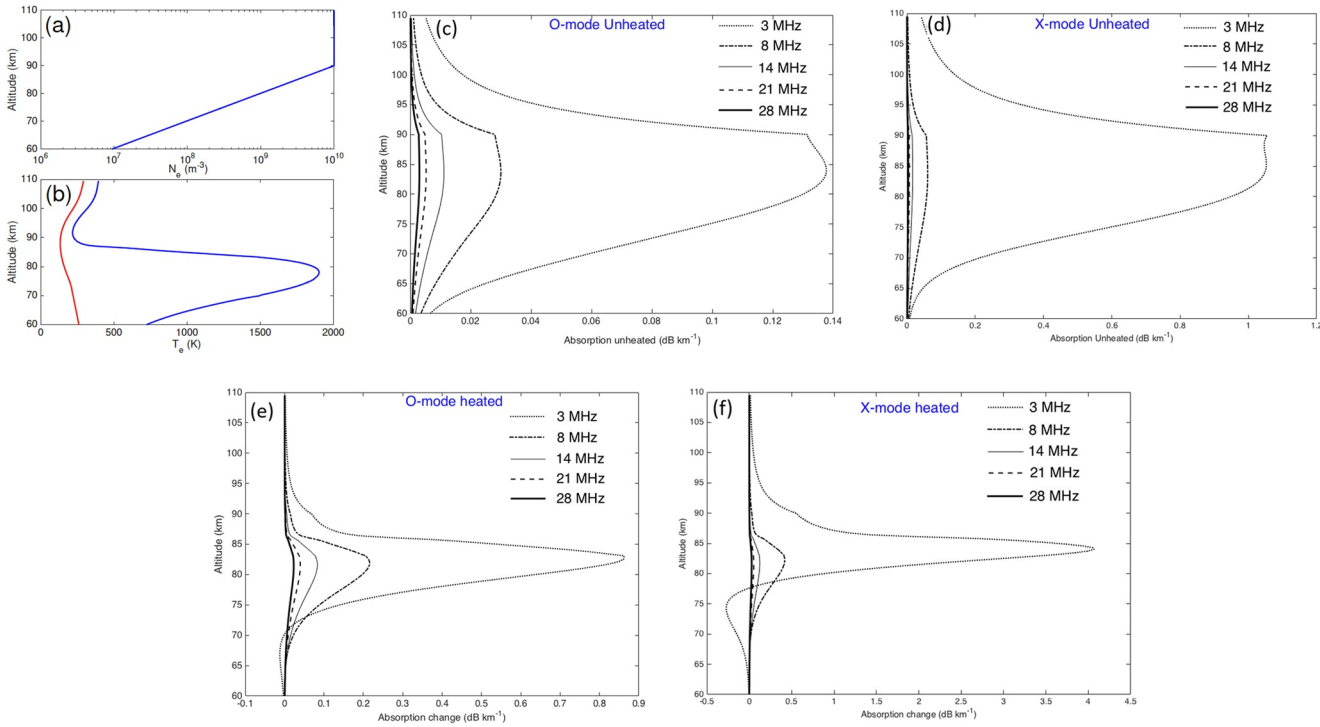

Figure 2. (a) Typical background electron density profile, (b) electron temperature profile (c, d) Absorption for the unheated mesospheric condition and differential absorption (dB km^{-1}) with respect to the heated ionosphere for transmission frequencies (f_0) of 3, 8, 14, 21, 28 MHz for O-mode and X-mode, respectively. (e, f) Similar to (c, d) for heated ionosphere.

Table 3
Total Absorption and Phase Variation of the Passing High-Frequency (HF) Signal Through the Natural and Artificially Modified Mesospheric Condition by High-Power HF Heating Wave for the O- and X-Mode Signals at f_0 = 3, 8, 14, 21, and 28 MHz

	Absorption O-mode	Absorption X-mode	Phase O-mode	Phase X-mode
3 MHz				
Unheated	1.917	11.582	1563.127	1559.207
Heated	7.609	24.044	1563.744	1562.733
8 MHz				
Unheated	0.454	0.894	4173.753	4173.264
Heated	2.421	4.238	4173.871	4173.529
14 MHz				
Unheated	0.173	0.256	7305 0.399	7305.241
Heated	1.034	1.474	7305 0.434	7305.298
21 MHz				
Unheated	0.082	0.107	10,958.680	010,958.610
Heated	0.519	0.666	10,958.693	10,958.628
28 MHz				
Unheated	0.048	0.059	1461 1.855	1461 1.816
Heated	0.310	0.375	1461 1.861	1461 1.824

O- and X-mode signals. The electron-neutral collision frequency is directly related to the neutral densities as (Schunk & Nagy, 1978):

$$\nu_{en} = 2.33\times10^{-17}N_2\left(1-1.21e^{-4}T_e\right)T_e + 1.82\times10^{-16}O_2\left(1+3.6e^{-2}\sqrt{T_e}\right)\sqrt{T_e} + 8.9\times10^{-17}O\left(1+5.7e^{-4}T_e\right)\sqrt{T_e} \quad (14)$$

Figure 3a represents the neutral densities of N_2, O_2, and O obtained from the MSIS model. The variation of absorption amplitude per kilometer for transmission frequencies of 16 and 28 MHz as a result of a neutral density increase by a factor of 2 is investigated. Figures 3b, 3d, and 3e show the variation of O- (blue lines) and X-mode (black lines) absorption (dB km^{-1}) as the neutral densities of N_2, O_2, and O are increased. A change of O_2 density by a factor of 2 makes a negligible impact on the absorption profile in the heated ionospheric plasma. A N_2 increase produces maximum absorption change by a factor of ~1.8 for both O- and X-modes. In the unheated ionosphere, O_2 and N_2 increased by a factor of 2 produce a notable change in the absorption profile versus altitude. Both frequencies show a similar trend for heated and unheated ionospheric plasma. In the unheated ionosphere and transmission frequency of 16 MHz, the maximum absorption amplitude changes from 0.0087 in the natural condition to 0.0105 and 0.0157 dB km^{-1} for the enhanced O_2 and N_2, respectively. It should be noted that an increase of O density by a factor of 2 does not affect the absorption amplitude with respect to the natural condition. A similar trend with a smaller variation is observed for the X-mode at 16 MHz. The main feature is that the unheated ionospheric condition shows a distinct behavior for increased background N_2, O_2, and O densities. Such a distinct effect is essential for the concept proposed in the following

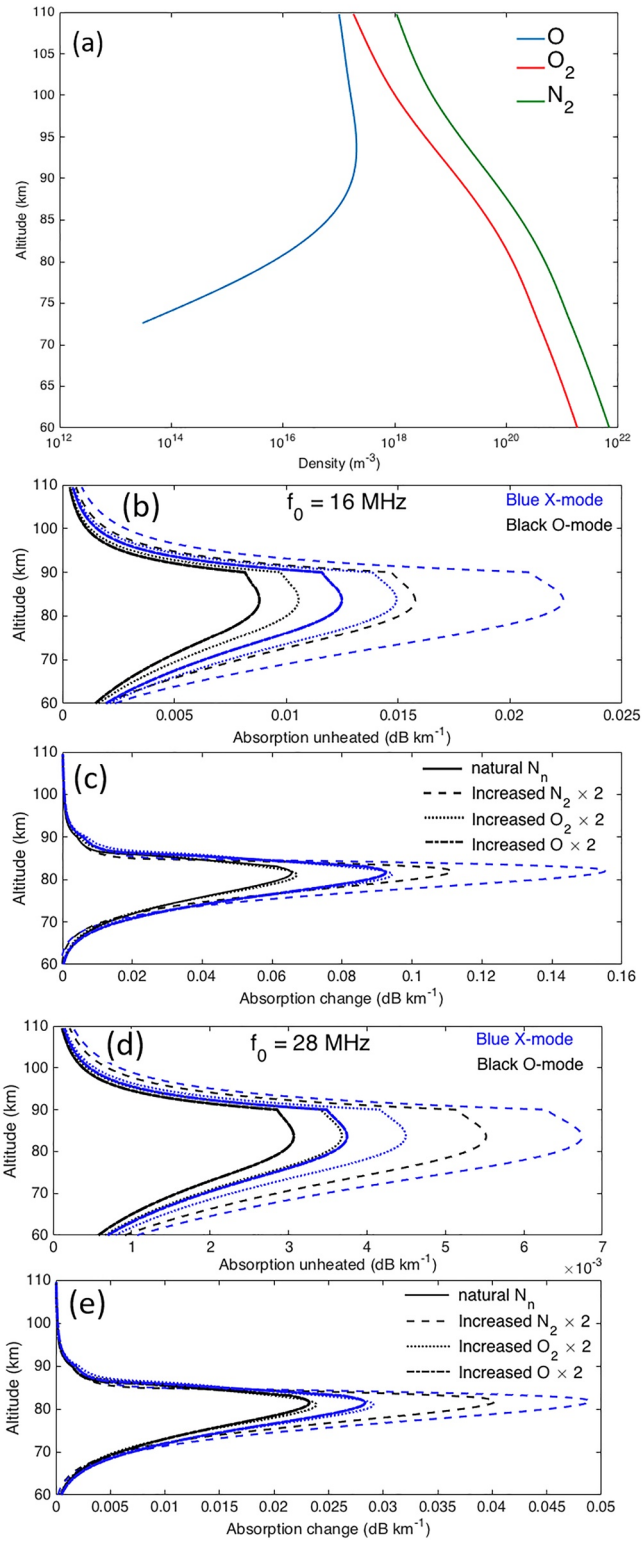

Figure 3. (a) Background neutral densities derived from MSIS model (b, c) The variation of the absorption at 16 MHz and (d, e) 28 MHz with varying neutral densities of N_2, O_2, O. The unheated ionospheric plasma conditions are shown in panels (b and d) Panels (c and e) represent the results for artificially heated ionospheric plasma.

section. Moreover, while elevated electron temperature will add additional information regarding the absorption change at different frequencies it alone can't provide the measurement of atmospheric constituents. More experimental observations are required to determine the best cooling model for estimation of HF absorption in the modified ionosphere using high-power HF radio-waves. Then, the absorption models and proposed technique in Section 5 can be implemented for possible D- and E-region measurements.

It should be noted that the technique introduced in this paper uses total absorption at each frequency and for different modes produced over the altitude range of 60–130 km. Therefore, a combination of experiments in both natural and heated ionospheric conditions could help to resolve unexpected atmospheric conditions.

3.2. Electron Density

Work by Senior et al. (2010) investigated the effect of the electron density variation on the absorption parameter. They have shown that maximum error produced in the absorption value as the electron density changes by a factor of 2 is of the order of 30%. Therefore, implementing more frequencies can eliminate such errors. Using other measurement sources for electron density such as Total Electron Content with ground GPS receivers or Ionosonde observations of the electron density profile would result in a more detailed calculation of D-region absorption. The phase data and Faraday rotation measurements at five frequencies could also lead to a more accurate measurement of TEC and make this approach self-consistent with other techniques discussed above.

The variation of absorption over the entire D-region for the O-mode in the heated (H) and natural (UH) ionosphere (ΔA_OH-UH), X-mode (ΔA_XH-UH), as well as differential absorption of O- and X-modes in the heated ionosphere (ΔA_{OX} H) and unheated (UH) ionosphere (ΔA_{OX} UH) for transmission frequencies of 8, 16, and 24 MHz are shown in Table 4. The main purpose of the proposed mission (called REEMA) is to measure the total absorption of the signal and also derive the ionospheric parameters, as well as extracting the neutral densities such as N_2, electron density, and temperature variation during radio wave heating of the ionosphere.

4. Machine Learning

The possibility of HF absorption observations on the ground using simultaneous multi-frequencies to determine background parameters in the D- and E-regions are explored in this section. Specifically, total absorption of a radio signal passing through the lower ionospheric region along with model simulation results of total absorption are incorporated to determine middle atmosphere temperature and composition. This includes both constituent and temperature observations that have a wide application in studying the physics and chemistry of the middle and upper atmosphere. A ML is developed to achieve this goal. A year of neutral atmosphere data from the MSIS model and electron density from the IRI model are used to educate the model. The selected data from 2019 are imported for absorption calculations using the model described in Sections 2 and 3. Then two days from 2018 to 2020 are selected to validate the model performance and accuracy.

The results for 2 days in a year before and after the trained database is used. Figures 5 and 6 show the ML results associated with 5 May 2018 and 2

Table 4
Detailed Study of Electron Density N_e and N_2 (as Dominant Neutral Constituent) on Associated Total Absorption at 8, 16, Is Presented

Typical			
	8 MHz		
ΔA_0(H-UH)	ΔA_X(H-UH)	ΔA_{0X}(UH)	ΔA_{0X}(H)
1.74	2.691	0.403	1.624
	16 MHz		
ΔA_0(H-UH)	ΔA_X(H-UH)	ΔA_{0X}(UH)	ΔA_{0X}(H)
0.619	0.841	0.052	0.274
	24 MHz		
ΔA_0(H-UH)	ΔA_X(H-UH)	ΔA_{0X}(UH)	ΔA_{0X}(H)
0.311	0.386	0.015	0.09
N2*2			
	8 MHz		
ΔA_0(H-UH)	ΔA_X(H-UH)	ΔA_{0X}(UH)	ΔA_{0X}(H)
2.116	3.281	0.672	1.837
	16 MHz		
ΔA_0(H-UH)	ΔA_X(H-UH)	ΔA_{0X}(UH)	ΔA_{0X}(H)
0.964	1.281	0.097	0.414
	24 MHz		
ΔA_0(H-UH)	ΔA_X(H-UH)	ΔA_{0X}(UH)	ΔA_{0X}(H)
0.441	0.541	0.028	0.128
Ne*2			
	8 MHz		
ΔA_0(H-UH)	ΔA_X(H-UH)	ΔA_{0X}(UH)	ΔA_{0X}(H)
2.498	4.026	0.882	2.183
	16 MHz		
ΔA_0(H-UH)	ΔA_X(H-UH)	ΔA_{0X}(UH)	ΔA_{0X}(H)
0.932	1.256	0.112	0.436
	24 MHz		
ΔA_0(H-UH)	ΔA_X(H-UH)	ΔA_{0X}(UH)	ΔA_{0X}(H)
0.425	0.523	0.032	0.13

February 2020, respectively. The diagram shown in Figure 4a represents the data assimilation implemented in this paper. A ML approach is adopted to evaluate the model performance to determine the atmospheric constituents, electron density, and neutral temperature. The data is collected every other day with hourly time resolution. A flow chart describing the ML approach is shown in Figure 4b. The total HF absorption at five frequencies (4, 8, 12, 16, and 20 MHz) are used to run the ML model and estimate the D and E-region constituents including N_2, O, O_2, as well as T and N_e. It should be noted that only total absorption data are incorporated in the ML model and the phase data, due to possible uncertainty in the actual observation, is excluded.

ML has been exploited to find the unknown constituents of D-layer according to the direct measurements of signal absorption for multiple frequencies in the HF band (4, 8, 12, 16, 20, and 24 MHz) and two modes (O and X). The procedure flowchart is shown in Figure 4b. For the learning process, T_e, N_e, and N_2, O_2, and O were captured from the IRI and MSIS models (TeL, NeL, nN2L, nOL, nO2L), respectively, for altitudes of 60–130 Km with 0.1 km resolution. The time resolution was hourly for 15 days in every month of the year 2019. After capturing these learning data, their proportional absorptions in O and X-mode for multiple frequencies (f) in the HF band (AL (TeL, NeL, nN2L, nOL, nO2L, mode, f)) were calculated according to the general form of the Appleton-Hartree

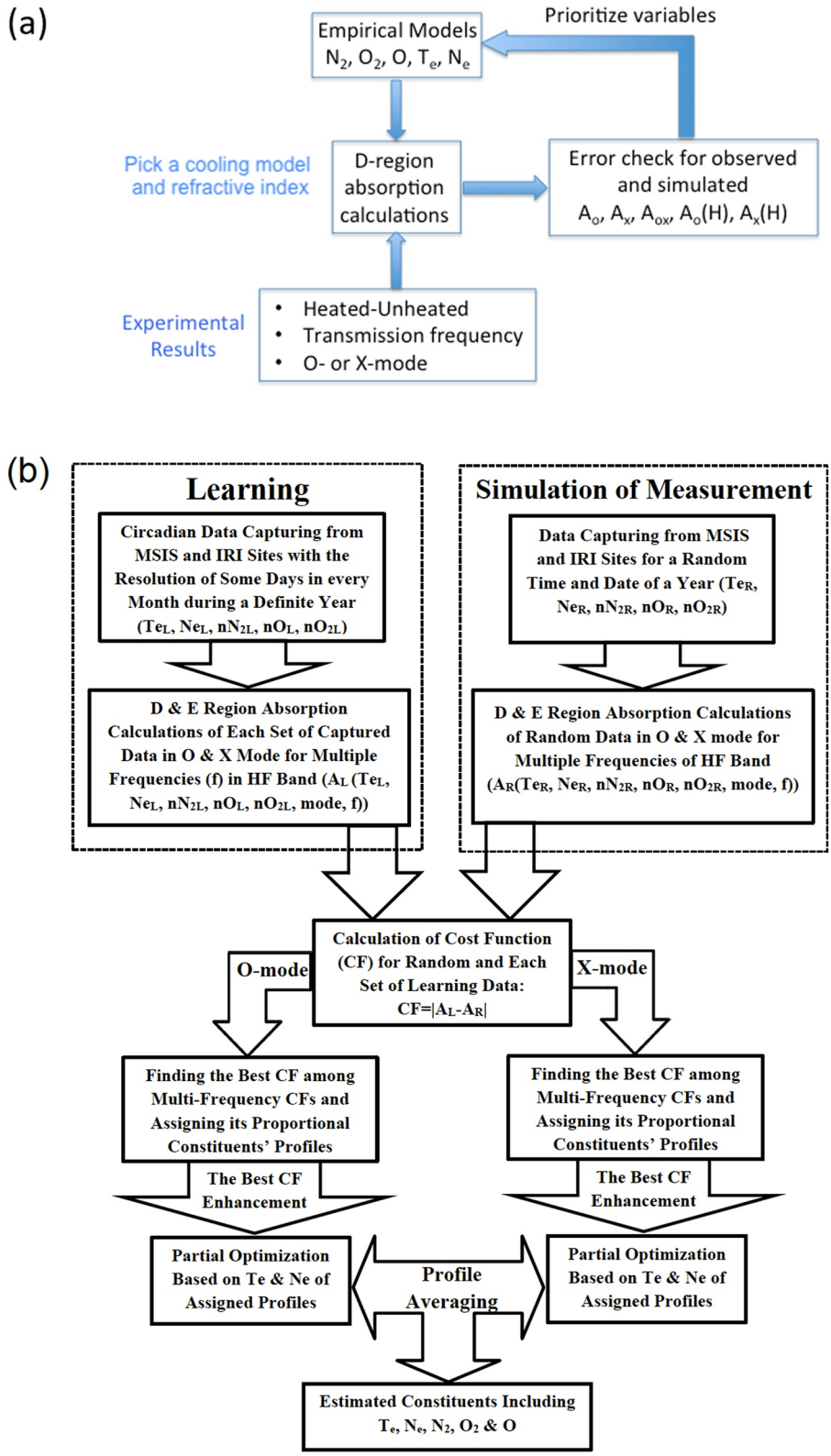

Figure 4. (a) Data assimilation diagram (b) machine learning procedure.

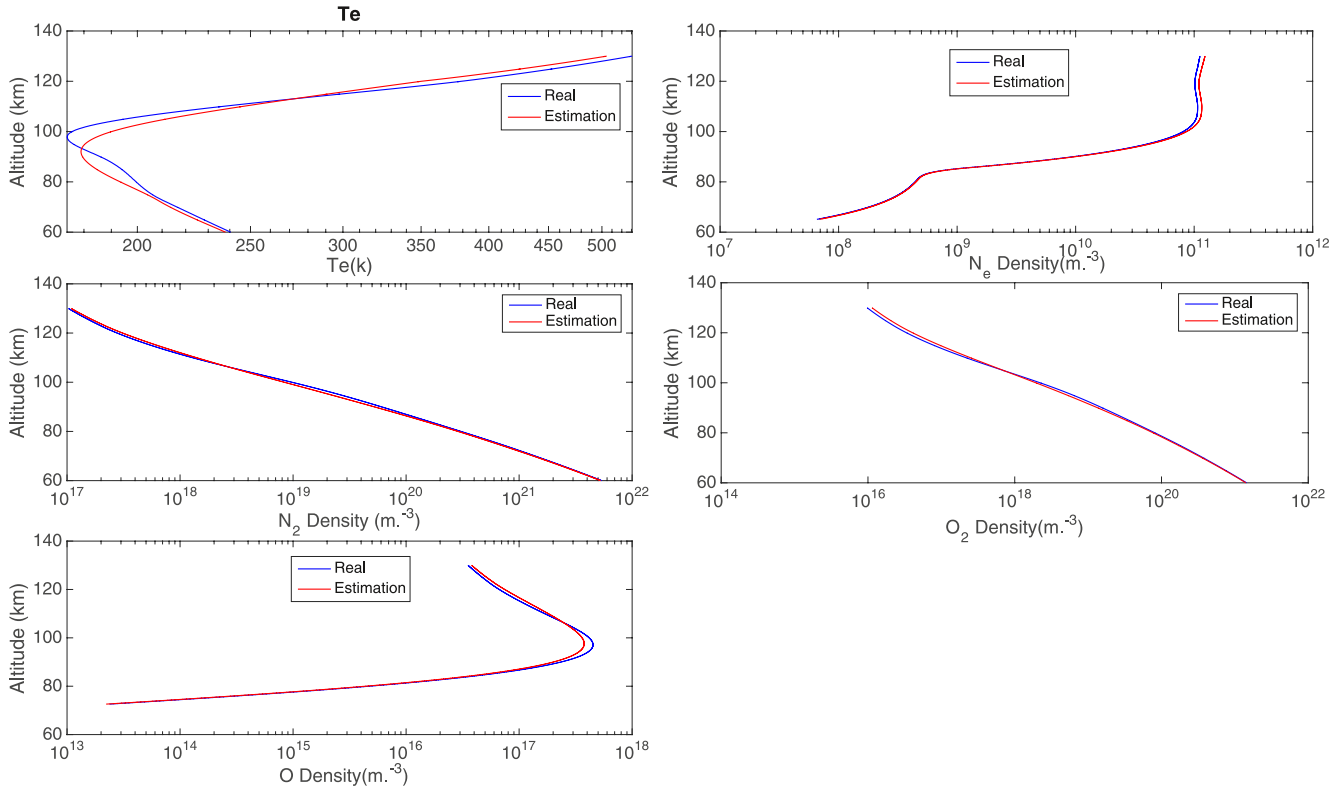

Figure 5. Machine learning (ML) results for 2 May 2018. The red line denotes the estimated results from ML model and blue line are the data obtained for the same date and time associated with the simulations.

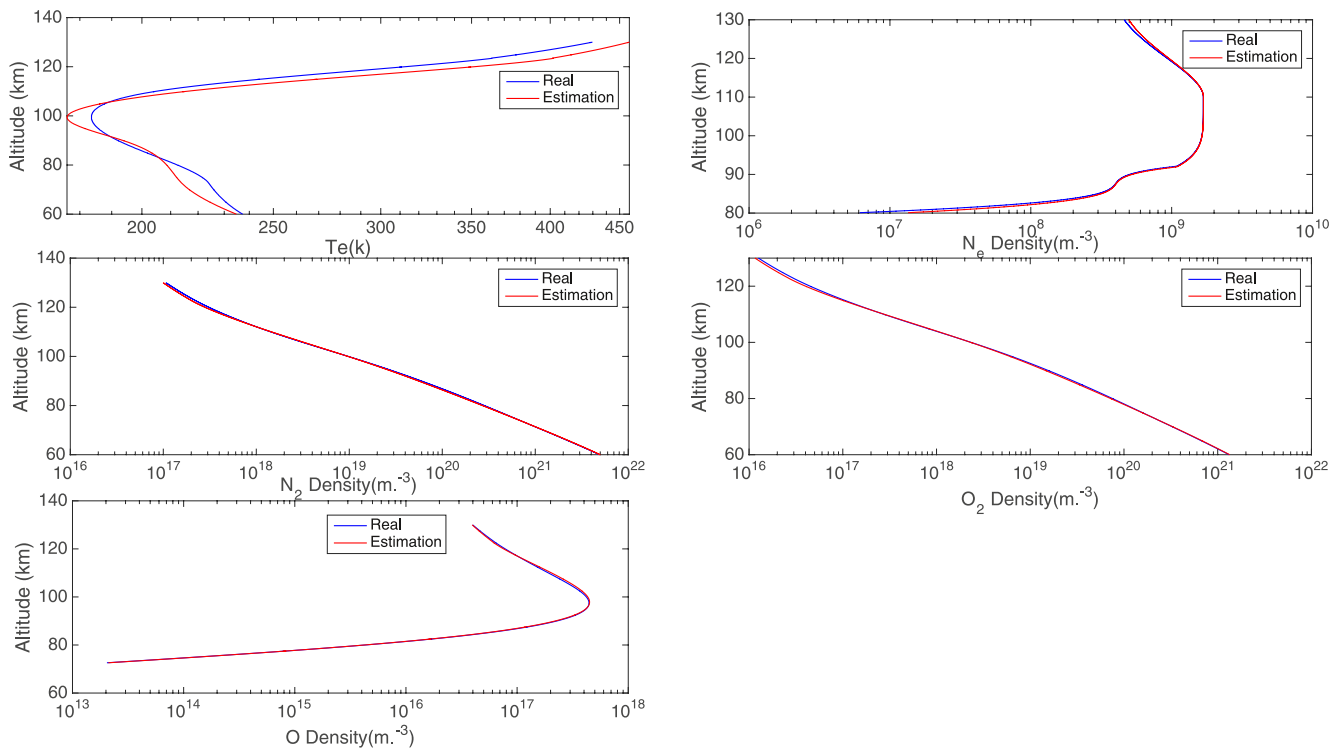

Figure 6. Machine learning (ML) results for 2 February 2020. The red line denotes the estimated results from ML model and blue line are the data obtained for the same date and time associated with the simulations.

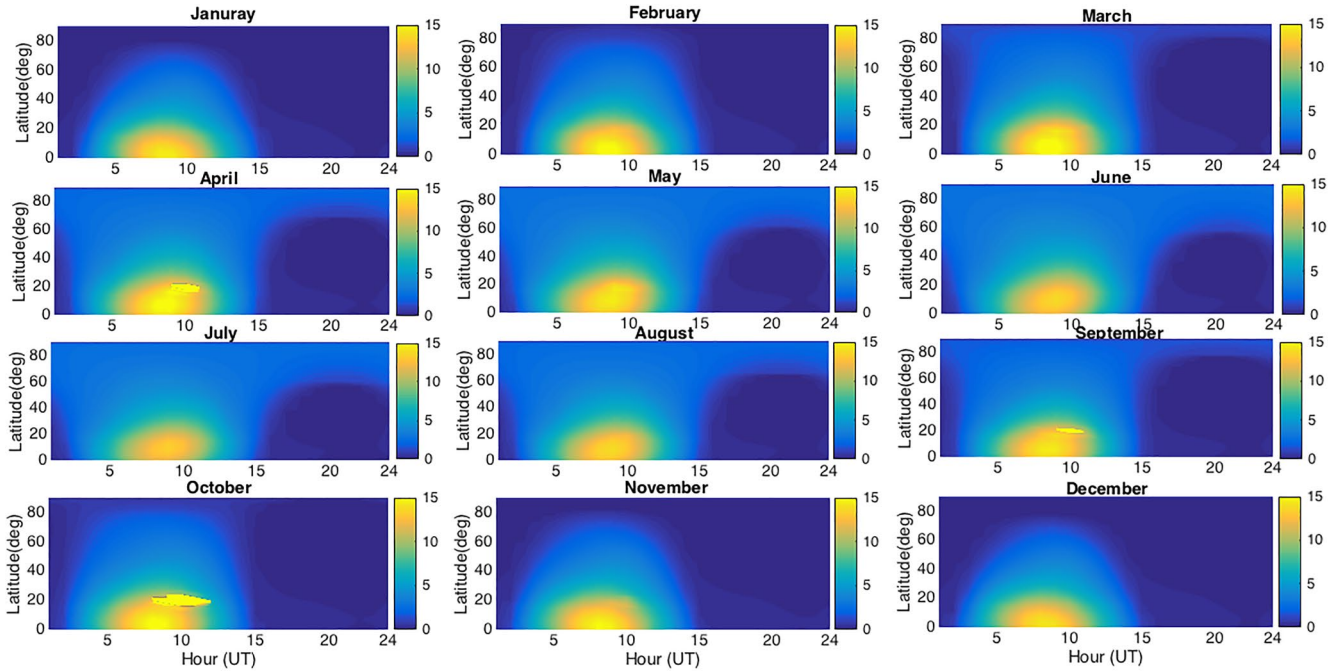

Figure 7. The global map of high-frequency (HF) absorption in the northern hemisphere associated with the empirical data obtained using MSIS and IRI models for 2019. The HF transmission with O-mode polarization at 4 MHz is used. A fixed longitude of 51.3347°E is used in the calculations. The color bar shows the total absorption in dB.

dispersion formula. In these calculations, the effect of the earth's magnetic field at all sampling altitudes and the collision frequency averaged over the electron velocity distribution function were taken into account. Thus, the collision frequency has been defined as an effective electron-neutral collision frequency as a function of the contributions for several different neutral species (Schunk & Nagy, 2009). To simulate the measurement setup, data capture from MSIS and IRI sites have been done for a random time and date of a year (TeR, NeR, nN2R, nOR, nO2R), then the same absorption calculation process as the learning step was performed AR (TeR, NeR, nN2R, nOR, nO2R, mode, f). The cost function (CF) was defined based on the absolute value of differences between the absorption of randomly sampled data and one of the learning datasets for multiple frequencies and two modes (CF = |AL − AR|). The CFs were processed in two distinct ways according to the modes. In each of them, the best (minimum) CF was found among the CFs of multiple frequencies. Subsequently, the proportional constituents' profiles according to the best CF were assigned to the estimated one. To enhance the best CF, that is, to minimize further, partial optimization based on T_e and N_e variations of the assigned profiles was done. Ultimately, the final estimated constituents' profiles were obtained by averaging two optimized constituents' profiles found for O/X modes.

The results for 2 days in a year before and after the trained database are used. The ML results are obtained in unperturbed ionospheric conditions. The days and hours selected to examine the ML results are out of the dates used to train the model. According to Figures 5 and 6, the error in the prediction of neutral densities including N_2, O, and O_2 is negligible. The neutral temperature profile shows agreement with the data. The altitude profile of estimated electron density matches well the original data used to calculate the corresponding total HF absorption at the selected frequencies. Implementing HF pump modulation will result in higher accuracy.

5. Global Mapping of HF Absorption in the Northern Hemisphere

To implement the technique described in Section 4, a global map of HF absorption needs to be generated. Distribution of ground HF receivers to monitor multi frequency total HF absorption is required to observe with high geographic coverage. Diurnal and monthly variations of total HF absorption in the northern hemisphere are presented. To calculate the HF absorption map in the northern hemisphere, a fixed longitude of 51.3347°E is used. Neutral densities are obtained from the MSIS model for the entire year. The data was collected in lati-

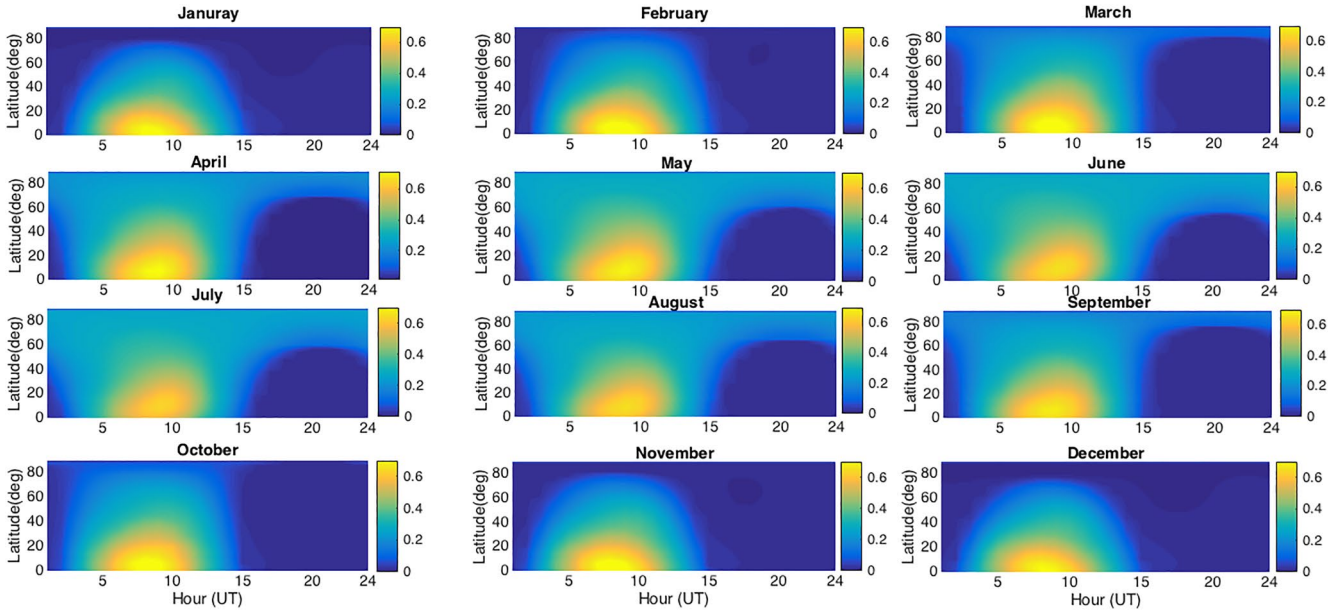

Figure 8. Similar to Figure 7 for 16 MHz.

tude range 0–90° with 1° resolution. The corresponding electron density was obtained from the IRI model. The empirical data are selected for 2019. The total absorption in the altitude range 70–140 km was calculated. The global map of HF absorption for O-mode propagation at 4 MHz is shown in Figure 7. The results are obtained in natural ionospheric condition without HF radio wave heating. From Figure 7, total absorption reaches 15 dB in the altitude range of interest. The global map in entire year shows a similar pattern with a maximum absorption extended in the latitude range of 0–20°. There is a small extension of high absorption to higher latitudes in the summer. For comparison, the observation associated with 16 MHz is presented in Figure 8. While the global pattern of HF absorption in the entire year remains similar to 4 MHz, the maximum absorption is reduced to 0.6 dB. The absorption for the X-mode is much higher in comparison with the O-mode (not shown). These results can be implemented to improve OTHR observations as well as oblique ionosonde soundings. Moreover, the technique described in Section 4 appears to be practical and sensitive to high latitudes.

6. Summary and Conclusions

In summary, the concept of developing a multi-frequency HF radio sounding technique for detailed measurement of the D-region absorption is investigated in this paper for the first time. The detailed calculations of absorption amplitude (dB km^{-1}) and total phase variation in the natural D-region ionosphere, as well as an artificially ionosphere pumped by a high-power radio wave, are considered. The HF absorption profiles and total HF absorption are calculated using the Garrett and Appleton-Hartree formula of refractive index. There is a small difference in estimated HF absorption between the two models, especially for unheated ionospheric conditions. The effect of three different cooling formulations associated with N_2 and O_2 vibrational and rotational excitation was found to be negligible in natural ionosphere. Performing such experiments in heated and unheated ionospheric plasma could be used to calibrate the instrument and to use the best cooling model and refractive index for the artificially modulated lower ionosphere.

The two O-mode and X-mode transmissions along with transmission frequencies of 2, 8, 16, 24, and 28 MHz associated with the proposed REEIMA HF beacon (Radio Explorer for Earth, Ionosphere, Mesosphere, and Atmosphere) are used to determine the absolute D-region absorption along with the possibility of estimating D-region parameters such as neutral densities. It has been shown that the variation of each background neutral density including N_2, O_2, and O produces a distinct effect on the absorption value of O- and X-mode as well as different transmission frequencies. A ML technique is developed based on the model simulation results using empirical data from the MSIS and IRI models for 2019. The accuracy of model appears to be encouraging for the estimation of the background temperature and neutral density profiles. Moreover, therefore, the proposed

technique can eliminate the effect of electron density variation and the possible error in OTHR measurement by using temporal evolution of HF absorption. Previous studies have shown that riometers may overestimate the absorption by a factor of 2 in the D-region ionosphere when modified by high-power radio waves despite changes in electron density and heater parameters.

A global map of HF absorption in the northern hemisphere associated with two transmission frequencies of 4 and 16 MHz are presented. It has been shown that diurnal and seasonal variation of global HF absorption is pronounced enough for such a technique to be implemented globally with a distributed network of HF receivers on the ground. The mission can be implemented to improve OTHR and SuperDARN observations in both hemispheres.

Appendix A: Garrett Formula of Refractive Index

The generalized refractive index (μ) of Garrett (1985) used in the calculations presented in this paper are presented in this section. The Equation 75 in Garrett (1985) is implemented as follow:

$$\mu^2 = 1 - \frac{AB - G^2}{B} - \frac{G^2\left(G^2 - B^2\right)}{BG^2 - \frac{1}{2}\frac{B-AB+G^2}{1-A+B}B^2\sin^2(\theta) \pm B^2\left[G^2\cos^2\theta + \frac{1}{4}\frac{B-AB+G^2}{1-A+B}\sin^4(\theta)\right]^2}$$

where A, B, and G are calculated as follow for the integration:

$$A = 0.5X\left(\prod_1 + \prod_2\right)$$
$$B = 0.5X\left(\prod_1 + \prod_2 - 2\prod_3\right)$$
$$G = 0.5X\left(\prod_1 - \prod_2\right)$$

In the above-mentioned expression the $\prod_1$ stands for complex nonlinear integral transform of $(1 - Y\omega)$, W, $\prod_2$ corresponds to complex nonlinear integral transform of $(1 + Y\omega, W)$, and $\prod_3$ refers to complex nonlinear integral transform of (ω, W). Where $\prod[\lambda, W(v)] = < \frac{1}{3v^2}\frac{d}{dv}\frac{v^3}{1-iW(v)/\lambda} >_v$, W corresponds to the wave energy, and $X = \Omega_{pe}/\omega$ and $Y = \Omega_{ce}/\omega$. The $\prod$ integral is calculated using quad function in MATLAB that approximates the integral of function from a to b using recursive adaptive Simpson quadrature. The real and imaginary parts of this integral are calculated.

Data Availability Statement

The model used in this paper is available through https://doi.org/10.5281/zenodo.7421195.

Acknowledgments
This work is supported by ISEF (Iran Saramadan Elmi Federation).

References

Bernhardt, P. A., & Huba, J. D. (1993). Reconstruction of non-stationary plasma irregularities using ionospheric tomography, cospar colloquia series: Low-latitude ionospheric physics.

Bernhardt, P. A., Huba, J. D., Chaturvedi, P. K., Fulford, J. A., Forsyth, P. A., Anderson, D. N., & Zalesak, S. T. (1993). Analysis of rocket beacon transmissions for computerized reconstruction of ionospheric densities. *Radio Science*, *28*(4), 613–627. https://doi.org/10.1029/93RS00383

Bernhardt, P. A., Huba, J. D., Selcher, C. A., Dymond, K. F., Carruthers, C. R., Bust, G., et al. (2001). New systems for space based monitoring of ionospheric irregularities and radio wave scintillations. In *Space weather, geophysical monograph* (Vol. 125, pp. 431–440). AGU.

Bernhardt, P. A., McCoy, R. P., Dymond, K. F., Picone, J. M., Meier, R. R., Kamalabadi, F., et al. (1998). Two dimensional mapping of the plasma density in the upper atmosphere with computerized ionospheric tomography (CIT). *Physics of Plasmas*, *5*, 2010–2021. https://doi.org/10.1063/1.872872

Bernhardt, P. A., Selcher, C. A., Siefring, C., Wilkens, M., Compton, C., Bust, G., et al. (2005). Radio tomographic imaging of sporadic E-layers during SEEK-2. *Annales Geophysicae*, *23*(7), 2357–2368. https://doi.org/10.5194/angeo-23-2357-2005

Bernhardt, P. A., & Siefring, C. L. (2006). New satellite-based systems for ionospheric tomography and scintillation region imaging. *Radio Science*, *41*(5), RS5S23. https://doi.org/10.1029/2005RS003360

Campbell, L., Brunger, M. J., Cartwright, D. C., & Teubner, P. J. O. (2004). Production of vibrationally excited N_2 by electron impact. *Planetary and Space Science*, *52*(9), 815–822. https://doi.org/10.1016/j.pss.2004.03.004

Caton, R., McNeil, W., Groves, K., & Basu, S. (2004). GPS proxy model for real-time UHF satellite communications scintillation maps from the Scintillation Network Decision Aid (SCINDA). *Radio Science*, *39*(1), RS1S22. https://doi.org/10.1029/2002RS002821

de La Beaujardiére, O. (2004). C/NOFS: A mission to forecast scintillations. *Journal of Atmospheric and Solar-Terrestrial Physics*, *66*(17), 1573–1591. https://doi.org/10.1016/j.jastp.2004.07.030

Evans, J. V. (1977). Satellite beacon contributions to studies of structure of the ionosphere. *Review of Geophysics*, *15*(3), 325–350. https://doi.org/10.1029/rg015i003p00325

Friedman, H. (1959). Rocket observations of the ionosphere. *Proceedings of the Institute of Radio Engineers*, *46*(2), 272–280. https://doi.org/10.1109/jrproc.1959.287294

Garrett, A. J. M. (1985). Multi species kinetic generalization of the Appleton-Hartree dispersion formula. *Journal of Plasma Physics*, *33*(2), 265–284. https://doi.org/10.1017/s0022377800002506

Garrett, A. J. M. (1991). Kinetic theory of cross modulation in a weakly ionized plasma. *Journal of Plasma Physics*, *46*(3), 365–390. https://doi.org/10.1017/s0022377800016196

Groves, K., Basu, S., Weber, E. J., Smitham, M., Kuenzler, H., Valladares, C., et al. (1997). Equatorial scintillation and systems support. *Radio Science*, *32*(5), 2047–2064. https://doi.org/10.1029/97rs00836

Havnes, O. (2004). Polar Mesospheric Summer Echoes (PMSE) overshoot effect due to cycling of artificial electron heating. *Journal of Geophysical Research*, *109*(A2), A02309. https://doi.org/10.1029/2003JA010159

Jackson, J. E. (1954). Measurements in the E layer with the Navy Viking rocket. *Journal of Geophysical Research*, *59*(3), 377–390. https://doi.org/10.1029/jz059i003p00377

Jones, D. B., Campbell, L., Bottema, M. J., & Brunger, M. J. (2003). New electron-energy transfer rates for vibrational excitation of O_2. *New Journal of Physics*, *5*, 114. https://doi.org/10.1088/1367-2630/5/1/114

Little, C. G., & Leinbach, H. (1959). The Riometer—A device for the continuous measurement of ionospheric absorption. *Proceeding of the IRE*, *47*, 315–320. https://doi.org/10.1109/JRPROC.1959.287299

Maeda, K. I. (1970). Radio propagation effects used on rockets in probing the ionosphere. *Journal of Atmospheric and Solar-Terrestrial Physics*, *32*(4), 647–661. https://doi.org/10.1016/0021-9169(70)90213-8

Mahmoudian, A., Kosch, M. J., Vierinen, J., & Rietveld, M. T. (2020). A new technique for investigating dust charging in the PMSE source region. *Geophysical Research Letters*, *47*(19), e2020GL089639. https://doi.org/10.1029/2020GL089639

Pavlov, A. V. (1998a). New electron energy transfer and cooling rates by excitation of O_2. *Annales Geophysicae*, *16*(8), 1007–1013. https://doi.org/10.1007/s00585-998-1007-8

Pavlov, A. V. (1998b). New electron energy transfer rates for vibrational excitation of N_2. *Annales Geophysicae*, *16*(2), 176–182. https://doi.org/10.1007/s00585-998-0176-9

Pavlov, A. V. (1998c). The role of vibrationally excited oxygen and nitrogen in the ionosphere during the undisturbed and geomagnetic storm period of 6–12 April 1990. *Annals of Geophysics*, *16*(5), 589–601. https://doi.org/10.1007/s00585-998-0589-5

Scales, W. (2004). Electron temperature effects on small-scale plasma irregularities associated with charged dust in the Earths mesosphere. *IEEE Transactions on Plasma Science*, *32*(2), 724–730. https://doi.org/10.1109/tps.2004.826082

Scales, W. A., & Mahmoudian, A. (2016). Charged dust phenomena in the near Earth space environment. *Reports on Progress in Physics*, *79*(10), 106802. https://doi.org/10.1088/0034-4885/79/10/106802

Schunk, R., & Nagy, A. (1978). *Ionospheres: Physics, plasma physics, and chemistry*. Cambridge University Press.

Schunk, R., & Nagy, A. (2009). *Ionospheres: Physics, plasma physics, and chemistry 2nd edition*. Cambridge University Press.

Seddon, J. C. (1953). Propagation measurements in the ionosphere with the aid of rockets. *Journal of Geophysical Research*, *58*(3), 323–335. https://doi.org/10.1029/JZ058i003p00323

Seliga, T. A. (1968). Analysis and results of low-frequency CW rocket propagation experiments in the D region. *Journal of Geophysical Research*, *73*(21), 6783–6794. https://doi.org/10.1029/JA073i021p06783

Senior, A., Mahmoudian, A., Pinedo, H., La Hoz, C., Rietveld, M. T., Scales, W. A., & Kosch, M. J. (2014). First modulation of high-frequency polar mesospheric summer echoes by radio heating of the ionosphere. *Geophysical Research Letters*, *41*, 5347–5353. https://doi.org/10.1002/2014GL060703

Senior, A., Rietveld, M. T., Honary, F., Singer, W., & Kosch, M. J. (2011). Measurements and modeling of cosmic noise absorption changes due to radio heating of the D region ionosphere. *Journal of Geophysical Research*, *116*(A4), A04310. https://doi.org/10.1029/2010JA016189

Senior, A., Rietveld, M. T., Kosch, M. J., & Singer, W. (2010). Diagnosing radio plasma heating in the polar summer mesosphere using cross modulation: Theory and observations. *Journal of Geophysical Research*, *115*(A9), A09318. https://doi.org/10.1029/2010JA015379

Smith, L. G., & Gilchrest, B. E. (1984). Rocket Observations of electron density in the nighttime E-region using Faraday-rotation. *Radio Science*, *19*(3), 913–924. https://doi.org/10.1029/rs019i003p00913